Auditory-inspired Interval Statistic Receivers for Passive Sonar Signal Detection

Robert W. Mill
Department of Computer Science
University of Sheffield
Sheffield, United Kingdom
Email: r.mill@dcs.shef.ac.uk

Guy J. Brown
Department of Computer Science
University of Sheffield
Sheffield, United Kingdom
Email: g.brown@dcs.shef.ac.uk

***Abstract*— The narrowband detector model used in passive sonars consists of a band-pass filter followed by a quadrature receiver, and so operates exclusively on signal power. The human ear suggests an alternative approach to narrowband detection based on signal phase, which is captured by phase locking in auditory nerve fibres. According to these principles, three "interval detectors"—detectors using information in zero crossing intervals—are developed and evaluated alongside a traditional power detector. The detectors all apply a maximum *a posteriori* criterion and assume Gaussian statistics. The power detector is shown to outperform the interval detector when the signal is centred on the analysis filter. When the signal frequency is displaced from the centre, interval detection improves and power detection worsens. Furthermore, a *critical displacement* exists, beyond which interval detectors are superior, and become useful for discriminating a weak signal in the filter tail.**

I. Introduction

A modern marine vessel houses a variety of equipment which, by virtue of periodic, mechanical processes, radiate an acoustic spectrum of discrete frequencies or tonals useful for target classification [1]. A detector may only operate on the basis of the signal received at a hydrophone array, which is invariably obscured by a number of broadband noise sources from the environment and the target itself [2], [3]. The conventional automated detector measures the power in a filtered signal and compares it to distributions conditioned on the hypothesis that the signal is present or absent, often on the assumption of additive Gaussian noise [4]. Here we present and evaluate three interval detectors, inspired by auditory processing, which detect a signal using information in the phase, rather than the envelope: specifically, the time interval between zero crossings.

The ear and brain together form the most advanced receiver and detector of acoustic signals found in nature. Narrowband passive sonars and the mammalian auditory system are similar in the sense that both resolve a wideband signal into sub-bands, facilitating the detection of narrowband components against a broadband noise background [3]. In the ear, the filtering stage is accomplished at the basilar membrane, which has a frequency-dependent response along its axis. The displacement of the basilar membrane is transduced into a neural signal by a lining of inner hair cells: the deflection of a hair cell produces an action potential, or "spike", which is communicated along the auditory nerve to the brain [5]. These spikes tend to occur in phase with the stimulus—a phenomenon referred to as phase-locking—so the frequency and modulation of the signal is preserved in the pattern of discharges.

Several studies attempt to capture the early stages of the auditiory pathway in an auditory model using a linear filter bank to model the vibration of the basilar membrane, and a zero crossing detector to reproduce phase-locking. Speech recognisers based on these models extract formant information from noise-corrupted speech signals more reliably than their Fourier-based counterparts [6]–[8]. Alongside experimental evidence, these approaches are justified on theoretical grounds. The zero crossing times of a narrowband signal constitute a non-uniform sampling of its phase [9] whose derivative reveals non-stationary components on a local time-frequency scale. A number of time-frequency distributions exploiting this principle have been developed in recent years [6], [10]–[12].

II. Preliminaries

This section briefly outlines the hypothesis testing and noise models common to all the detectors described in Section III. Literature pertaining to random processes varies in its terms and notation, so these are defined explicitly.

A. Hypothesis Testing

Starting with a sampled signal $x[t]$, a detector must choose between $M+1$ hypotheses, labelled $H_0, \ldots, H_M$, on the basis of a test statistic, $\mathbf{s}$, derived from the observed data. For a maximum *a posteriori* detector, H_j is chosen according to

$$\underset{j}{\operatorname{argmax}}\, p(\mathbf{s}|H_j)P(H_j), \tag{1}$$

where $p(\mathbf{s}|H_j)$ is a conditional probability density function and $P(H_j)$ is a prior probability. Such a detector provides optimum performance for the test statistic, when incorrect decisions carry equal cost and the conditional probability functions accurately model the true distributions. All the detectors presented in this paper adopt the maximum *a posteriori* criterion.

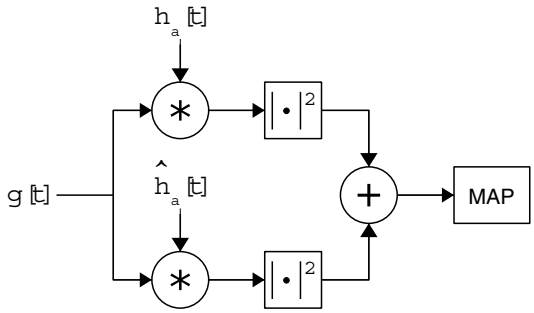

Fig. 1. The squared-envelope detector squares and sums the in-phase and quadrature signal components, obtained by convolution with $h_a[t]$ and $\hat{h}_a[t]$, and applies a maximum *a posteriori* (MAP) decision rule.

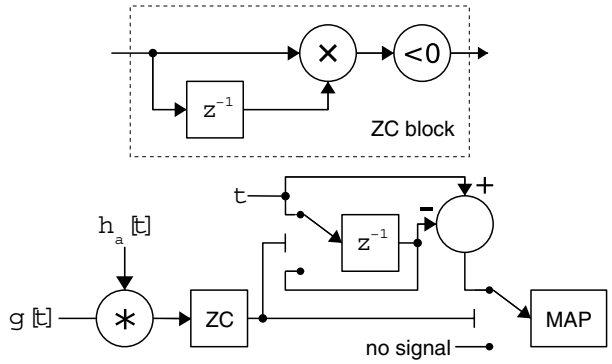

Fig. 2. Zero crossing detector (upper) and elementary interval detector (lower). The ZC block is a zero crossing subsystem; the switches connect to the upper pathway when their condition (⊣) is positive.

B. Noise Model

Let us assume that each hypothesis H_j is associated with a zero mean, wide-sense stationary Gaussian process. For any of these processes X, the following conditions apply:

$$E\{x_t\} = 0 \quad (2)$$

$$E\{x_t x_{t-\tau}\} = \gamma_j[\tau] \quad (3)$$

$$(x_{t_1}, x_{t_2}, \ldots, x_{t_N}) \sim \mathcal{N}_N\{0, \Sigma_{t_1,\ldots,t_N}\} \quad (4)$$

where we abbreviate $X(t) \equiv x_t$. Condition (3) requires that the autocovariance $\gamma[\tau]$ be time invariant, i.e., a function of lag τ only. Condition (4) indicates that any selection of samples is governed by a joint Gaussian distribution, whose covariance matrix Σ depends on the separation of the time instants. The entries σ_{ij} of Σ must satisfy

$$\sigma_{ii} = \sigma^2 = \gamma[0] \quad (5)$$

$$\sigma_{ij} = \sigma_{ji} < \sigma^2, \ \forall i \neq j. \quad (6)$$

The autocorrelation $\rho[\tau]$ and power spectral density $S[\omega]$ are related to the above quantities by

$$\rho[\tau] = \gamma[\tau]/\gamma[0] \quad (7)$$

$$S[\omega] = \mathrm{DFT}\{\gamma[\tau]\} \quad (8)$$

where $\mathrm{DFT}\{\cdot\}$ denotes a discrete Fourier transform operation, and (8) is a statement of the Wiener-Khinchin theorem [13].

III. Detectors

The four detectors described next receive an input signal $g[t]$ and pass it through an analysis filter with impulse response $h_a[t]$. The following discussion considers only the filtered signal $x[t] = h_a[t] * g[t]$.

A. Squared Envelope Detector

The test statistic used by this detector is a single sample of the squared envelope within the analysis channel. Denote the output of the analysis channel $x[t]$, and its quadrature, obtained by means of the Hilbert transform, $\hat{x}[t]$. The test statistic measured at time t_s is

$$a = x^2[t_s] + \hat{x}^2[t_s].$$

The random process associated with hypothesis H_j has an autocovariance $\gamma_j[\tau]$. The squared envelope is governed by an exponential distribution [4], whose probability density function is

$$p_A(a|H_j) = \frac{1}{2\gamma_j[0]} \exp \frac{-a}{2\gamma_j[0]}. \quad (9)$$

So a minimum error binary detector chooses H_1 iff

$$\frac{\gamma_0[0]}{\gamma_1[0]} \exp\left(-\frac{a}{2}\left[\frac{1}{\gamma_1[0]} - \frac{1}{\gamma_0[0]}\right]\right) > 1.$$

A block diagram of the squared-envelope detector is provided in Fig. 1.

B. Elementary Interval Detector

The test statistic used by the elementary interval detector is the duration of a zero crossing interval, in samples, formed by counting the samples between the zero crossings. For instance, the pattern of sign changes $(-,+,+,+,-)$, provides the test statistic i=3. Values for i are only available at zero crossings. The elementary interval detector is illustrated schematically in Fig. 2.

Let the random variable I represent the duration of a zero crossing interval. The cumulative distribution function for I conditioned on hypothesis H_j has the approximation [14]

$$P(i \leq I|H_j) \approx \quad (10)$$

$$\begin{cases} 0 & i \leq 0 \\ \frac{1}{2} + \frac{\sin^{-1}\rho_j[i+1] - \sin^{-1}\rho_j[i]}{\pi - 2\sin^{-1}\rho_j[1]} & 0 < 2i < f_s/f_c \\ 1 & \text{otherwise,} \end{cases}$$

subject to an octave band-limitation requirement

$$S_j[2\pi f] \approx 0, \ f_c < f < 2f_c,$$

for sample rate f_s Hz and lower cut-off frequency f_c Hz. The corresponding probability density function is found by differencing (10) in the usual manner:

$$p_I(i|H_j) = P(i \leq I|H_j) - P(i < I|H_j). \quad (11)$$

The decision rule for the elementary interval detector is obtained by placing (11) into (1). The probability of error (excluding model error) may be determined directly from the cumulative distribution functions.

C. Continuous Interval Detector

The elementary interval detector places zero crossings at the mid-point between sign changes when computing the test statistic i. The resultant round-off error appreciably reduces performance, even at frequencies as low as $\approx 0.02 f_s$. The continuous interval detector enhances performance at higher frequencies by modelling the signal in continuous time.

The test statistic used by the continuous interval detector is derived from the time difference between zero crossings obtained via interpolation. In this study, we adopt a linear interpolation, i.e., for two sample values x_t and x_{t+1} the zero crossing time t_z is given by

$$t_z = t + \frac{x_t}{x_t - x_{t+1}}.$$

For instance, the sequence $(-0.1, 0.1, 0.5, 0.2, -0.4)$ yields the test statistic $i_c = 2.8\dot{3}$, which is more precise than $i = 3$.

As the test statistic i_c is continuous, it remains to convert the probability density functions in the decision rule into a continuous form. Starting with the cumulative distribution for I in (10), we take a limit as the sampling interval $\triangle i$ tends to zero:

$$P(i_c \leq I_c | H_j) \approx \lim_{\triangle i \to 0} \left\{ \frac{1}{2} + \frac{\sin^{-1} \rho_j(i_c + \triangle i) - \sin^{-1} \rho_j(i_c)}{\pi - 2 \sin^{-1} \rho_j(\triangle i)} \right\}. \tag{12}$$

where $\rho[i] \equiv \rho(i \cdot \triangle i)$. This can be manipulated into the form

$$\frac{1}{2} + \frac{1}{2\pi} \lim_{\triangle i \to 0} \left\{ \frac{\triangle i \cdot (\sin^{-1} \rho_j(i_c + \triangle i) - \sin^{-1} \rho_j(i_c))}{\triangle i \cdot (\frac{1}{2} - \frac{1}{\pi} \sin^{-1} \rho_j(\triangle i))} \right\} \tag{13}$$

and separated into a product of limits

$$\frac{1}{2} + \frac{1}{2\pi} \lim_{\triangle i \to 0} \left\{ \frac{\triangle i}{\frac{1}{2} - \frac{1}{\pi} \sin^{-1} \rho_j(\triangle i)} \right\} \times \lim_{\triangle i \to 0} \left\{ \frac{\sin^{-1} \rho_j(i_c + \triangle i) - \sin^{-1} \rho_j(i_c)}{\triangle i} \right\}. \tag{14}$$

The first limit converges to the reciprocal of Rice's Formula [15]; the second limit may be recognised as differentiation from first principles. After making suitable replacements, we arrive at the cumulative distribution function with a continuous argument,

$$P(i_c \leq I_c | H_j) \approx \frac{1}{2} + \frac{\rho_j'(i_c)}{2\sqrt{\rho_j''(0)(\rho_j^2(i_c) - 1)}}. \tag{15}$$

The probability density function is found by differentiating (15) with respect to i, which gives

$$p_{I_c}(i_c) \approx \frac{(\rho_j^2(i_c) - 1)\rho_j''(i_c) - \rho_j(i_c)(\rho_j'(i_c))^2}{2\sqrt{\rho_j''(0)}(\rho_j^2(i_c) - 1)^{3/2}}. \tag{16}$$

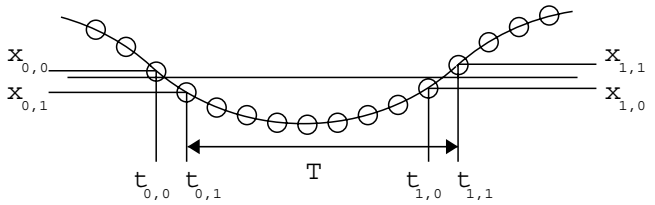

Fig. 3. Zero crossing times $t_{i,j}$, values $x_{i,j}$ and sample separation T.

As a final note, when considering the interval output of a linear system with Gaussian noise input, it is useful if the impulse response of every block in the system is expressible as a modulated-Gaussian mixture (MGM), which we define to be

$$\sum_{k=1}^{N} A_k e^{-2(C_k t)^2} e^{j(\omega_k t + \phi_k)}, \tag{17}$$

where A_k, $C_k > 0$, ω_k, ϕ_k are constants. Under these conditions, it may be shown that $\gamma_j(\tau)$, $\rho_j(\tau)$ and $S_j(\tau)$ have MGM form, and that (15) and (16) have a closed form. The integral and square-integral of a MGM over $(-\infty, \infty)$ also has a closed form (a constant), which facilitates the direct computation of helpful quantities, such as process output power.

D. Interpolated Interval Detector

The interpolated interval detector resembles the continuous interval detector, insofar as it accounts for fractional zero crossing times; however, instead of employing continuous functions, the interpolated detector explicitly models the zero crossings arising from a linear interpolation in discrete time.

In this section, we define an interval as two zero crossings separated by T samples. Each zero crossing contains two samples, and an interval contains four samples

$$\mathbf{x} = (x_{0,0}, x_{0,1}, x_{1,0}, x_{1,1}).$$

The subscripts on x respectively index the crossing and sample, as illustrated in Fig. 3. The distribution governing $\mathbf{x}$ is joint Gaussian and has the density function

$$p_{\mathcal{X}}(\mathbf{x}|H_j) = \frac{1}{4\pi^2 |\Sigma_{\mathcal{X}}|^{1/2}} \exp\left(\frac{\mathbf{x}^T \Sigma_{\mathcal{X}}^{-1} \mathbf{x}}{-2} \right) \tag{18}$$

with the covariance matrix (scaled to unit variances)

$$\Sigma_{\mathcal{X}} = \begin{pmatrix} 1 & \rho_j[1] & \rho_j[T] & \rho_j[T+1] \\ \rho_j[1] & 1 & \rho_j[T-1] & \rho_j[T] \\ \rho_j[T] & \rho_j[T-1] & 1 & \rho_j[1] \\ \rho_j[T+1] & \rho_j[T] & \rho_j[1] & 1 \end{pmatrix}. \tag{19}$$

As we are in possession of the autocorrelation function $\rho_j[\cdot]$, $\Sigma_{\mathcal{X}}$ can be filled out appropriately, and hence $p_{\mathcal{X}}(\mathbf{x})$ is known completely.

The algorithm utilises the fractional zero crossing times, z_0 and z_1, rather than sample values. Whilst the values for $x_{i,j}$ are hidden, it is known that

$$z_j = \frac{x_{j,0}}{x_{j,0} - x_{j,1}}, \; x_{j,0} \neq x_{j,1}, \tag{20}$$

or,

$$x_{j,1} = x_{j,0}\left(1 - \frac{1}{z_j}\right). \tag{21}$$

Equation (21) shows that knowledge of a zero crossing time establishes a homogeneous, linear relationship between the two samples. From this, we know that a pair of zero crossing times corresponds to a plane passing through the $\mathcal{X}$ space, which itself has four dimensions. The inclination of this plane is given by θ_0 and θ_1, related to the zero crossing times by

$$\theta_j = \arctan(1 - 1/z_j). \tag{22}$$

Subjecting the probability space $\mathcal{X}$ to the scale-invariant rotation associated to the matrix

$$A = \begin{pmatrix} \cos\theta_0 & \sin\theta_0 & 0 & 0 \\ -\sin\theta_0 & \cos\theta_0 & 0 & 0 \\ 0 & 0 & \cos\theta_1 & \sin\theta_1 \\ 0 & 0 & -\sin\theta_1 & \cos\theta_1 \end{pmatrix} \tag{23}$$

creates a transformed probability space $\mathcal{Y}$ with covariance matrix

$$\Sigma_{\mathcal{Y}} = A\Sigma_{\mathcal{X}}A^T. \tag{24}$$

In $\mathcal{Y}$-space, events corresponding to a pair of zero crossings $\langle z_0, z_1\rangle$ lie on the plane

$$y_{0,1} = y_{1,1} = 0. \tag{25}$$

The plane itself has no probability mass. In order to point condition, one must consider the probability mass residing in the region $[0, \delta\theta_0], [0, \delta\theta_1]$. To effectively integrate this region, a change of variables to another space $\mathcal{Z}$ is required, using

$$y_{0,0} = R_0\cos\phi_0, \quad y_{0,1} = R_0\sin\phi_0,$$
$$y_{1,0} = R_1\cos\phi_1, \quad y_{1,1} = R_1\sin\phi_1,$$

which has Jacobian $|R_0R_1|$. Changing the variables, setting $\phi_j = 0$, and adding the Jacobian factor to the $\mathcal{Y}$ pdf gives

$$p_{\mathcal{Z}}(R_0, R_1) = \frac{R_0R_1}{4\pi^2|\Sigma_{\mathcal{Y}}|^{1/2}} \exp\left(\frac{\kappa_{1,1}R_0^2 + \kappa_{3,3}R_1^2 + 2\kappa_{1,3}R_0R_1}{-2}\right) \tag{26}$$

where κ_{ij} is the (i,j)-th element of $\Sigma_{\mathcal{Y}}^{-1}$. Observe that the majority of exponentiated terms in (26) disappear due to $\sin\phi = 0$. The variables R_0 and R_1 may be interpreted as either Cartesian co-ordinates on the zero crossing plane, or, alternatively, the magnitudes in two polar planes. We want to include the probability mass in the entire zero crossing plane, i.e., integrate

$$\int_0^\infty \int_0^\infty p_{\mathcal{Z}}(R_0, R_1) dR_0 dR_1. \tag{27}$$

The integral in (27) has a solution in closed form. The procedure for obtaining it is lengthy and not documented here. (See [14] for details.) At a descriptive level, the variables R_0 and R_1 are transformed so that $\kappa_{1,3} = 0$ and $\kappa_{1,1} = \kappa_{3,3} = 1$, (i.e., decoupled using an Eigenvalue decomposition), then the integrand is changed to polar coordinates and the bounds re-calculated prior to integration.

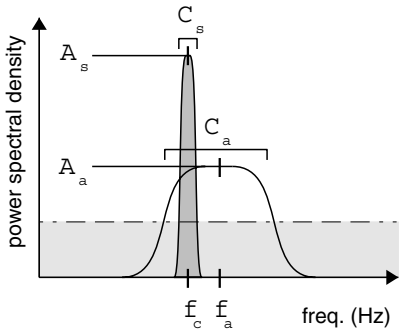

Fig. 4. Schematic illustration showing how the quantities A, C and f relate to the power spectra. The signal and noise power are equivalent to the dark and light gray areas, respectively.

IV. Results

To evaluate the four detectors, each was applied to the task of detecting a narrowband noise signal in broadband noise. The performance metric adopted was the probability of error (PE). This study investigated how the PE varied with i) signal to noise ratio (SNR); ii) signal frequency in relation to band centre; and iii) analysis centre frequency. In the case of the envelope, elementary and continuous detector, the PE can be predicted analytically, so the empirical measurements serve to validate the working. The performance of the interpolated interval detector is more difficult to compute analytically and only empirical results are reported.

A. Method

The target signal is a narrow band of noise formed by convolving white Gaussian noise with the impulse response

$$h_s[t] = A_s e^{-2(C_s t)^2}\cos 2\pi f_c t/f_s \tag{28}$$

where C_s controls bandwidth, f_c is the centre frequency in Hz, f_s is the sample rate (16384 Hz), and A_s is adjusted to scale the impulse response so that the signal power is σ_s^2. Notched noise is used rather than a sinusoid, as the former is a Gaussian process. The noise signal is white Gaussian noise with noise power σ_n^2. The global signal-to-noise ratio is defined by

$$\text{SNR} = 10\log_{10}\frac{\sigma_s^2}{\sigma_n^2},\ \text{dB}. \tag{29}$$

The analysis filter has the impulse response

$$h_a[t] = A_a e^{-2(C_a t)^2}\cos 2\pi f_a t/f_s$$

where, A_a, C_a and f_a similarly control gain, bandwidth and centre frequency—see Fig. 4.

Two artificial signals are created: the first by passing noise through the analysis filter, corresponding to H_0, the other by passing both signal and noise through the analysis filter, corresponding to H_1. The empirical PE is determined by counting the correct and incorrect classifications made by each detector for H_0 and H_1.

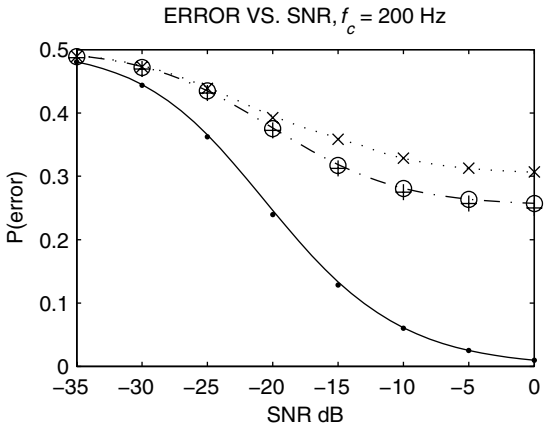

(a) Signal frequency at 200Hz (on-centre)

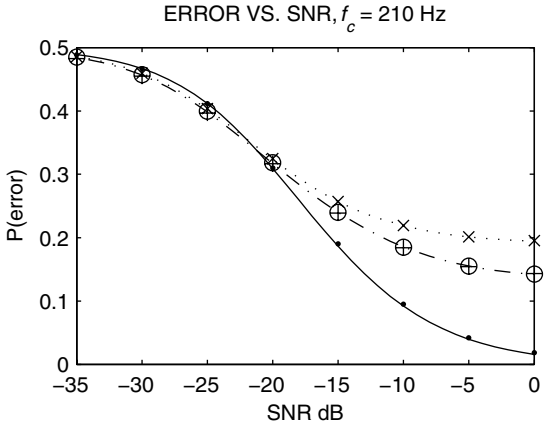

(b) Signal frequency at 210Hz (off-centre)

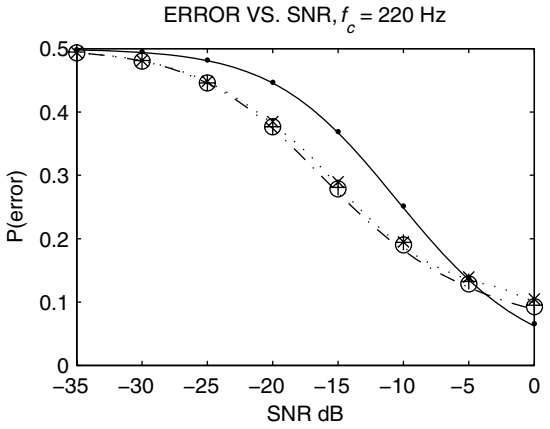

(c) Signal frequency at 220Hz (further off-centre)

Fig. 5. Probability of error as a function of SNR. The curves show the analytical predictions regarding performance for the power (solid), elementary interval (dotted) and continuous interval detectors (dash-dotted). The empirical results are plotted as markers for the power (•), elementary (×), continuous (○) and interpolated (+) detectors.

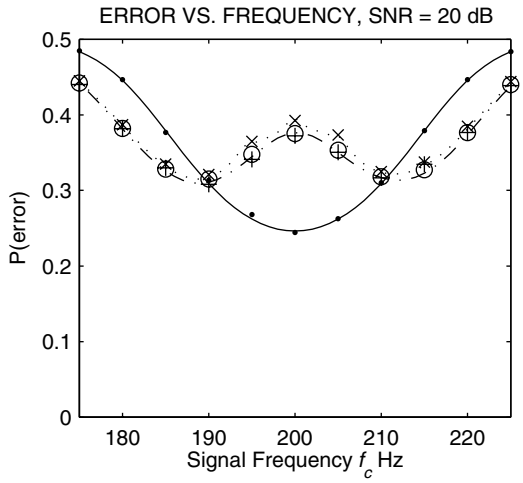

Fig. 6. Probability of error as a function of signal frequency, designed to show the effect of changing the signal frequency in relation to the band centre. In this case, the band is centred on 200 Hz and the SNR is -20 dB. Refer to the caption of Fig. 5 for the legend.

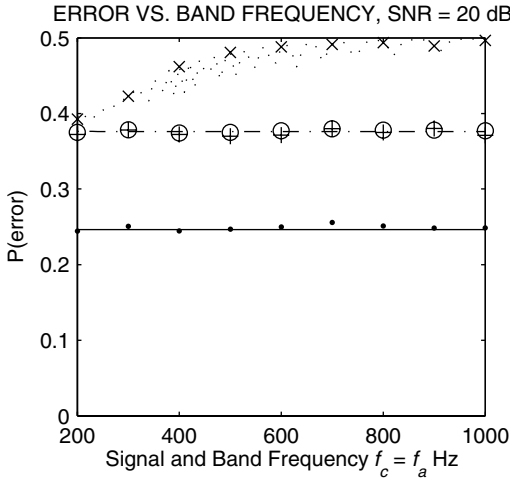

Fig. 7. Probability of error as a function of signal and band centre frequency varied together. The signal frequency falls at the band centre in every condition. Refer to the caption of Fig. 5 for the legend.

B. Analysis of Results

The first experiment examined the relationship between the signal-to-noise ratio and the probability of error, using the values f_c=200, C_s=10, f_a=200, C_a=40. Note that the signal was centred on the analysis band. The PE for each detector is plotted in Fig. 5(a) as function of SNR. The predicted performance of the detectors are shown as curves; the markers show empirical measurements obtained from half a million Monte Carlo trials. The PE monotonically decreases with SNR, as one would expect, and the agreement between the predicted and observed values validate the working in Section III. The power detector consistently outperforms the interval detectors by a wide margin, whilst the continuous and interpolated detectors achieve a slight performance gain over the elementary detector.

The second experiment investigated the effect of changing the signal frequency in relation to the band centre. The experiment described above was repeated with a change in the parameter: f_c=210 Hz and f_c=220 Hz, producing the results shown in Figs. 5(b) and 5(c), respectively. The shift in frequency dramatically alters the transition curves: for 210 Hz, the detectors perform similarly at low SNRs; for 220 Hz, the interval detectors outperform the power detector. To study this effect in detail, a plot of PE against f_c was generated with the SNR held fixed at -20 dB, the results of which are shown in Fig. 6. We note some interesting behaviour:

1) Centred: When the signal coincides with the analysis band frequency, then the maximum signal energy is passed and the conditional mean powers are well-separated. On the other hand, the conditional mean *intervals* under each hypothesis are extremely close, and only the difference in variance can distinguish the two.

2) Off-centre: When the signal is shifted some distance from the band centre, the signal power is reduced, so that the conditional mean powers are drawn together. At the same time, the presence of an off-centre signal causes the conditional mean intervals to move apart, improving the quality of the test.

We refer to the frequency offset required for the interval detectors to outperform the power detector as the *critical displacement*. Fig. 6 shows that the critical displacement for a band centred on 200 Hz and SNR at -20 dB is 10 Hz.

The third experiment investigated the effect of increasing both the signal and analysis frequencies. Interval detectors rely upon accurate estimates of zero crossing times; the elementary interval detector introduces severe round-off error (cf. Section III-C) at high frequencies, which the continuous and interpolated interval detectors are designed to overcome. Experiment three effectively demonstrates the success of these enhancements. Fig. 7 confirms that the PE of the elementary interval detector rises with increasing frequency, whilst the PE of the continuous and interpolated interval detectors remain constant.

V. Conclusions and Future Work

Three interval detectors and a power detector were required to detect the presence of a narrowband signal against a white noise background. The signal-to-noise ratio, signal frequency and analysis band were all varied, and the effect upon the probability of error for each detector was examined. The results may be summarised as follows. First, the observed and predicted performance (where available) of each detector are in close agreement, indicating the absence of model error. Second, the probability of error for the power and interval detectors depend upon the frequency of the signal in relation to the band centre frequency. Third, in order to provide admissable performance at higher frequencies, the interval detector requires a finer temporal resolution than simply rounding to the nearest sample affords. It is shown that constructing a detector using continuous interval distributions, or distributions which account directly for linear interpolation, are both appropriate solutions.

This study considered the particular case of minimum error, binary detection in a white Gaussian noise signal. It may be noted that the techniques described are more general, and are readily extensible to other Bayesian-derived decision criteria (e.g., Neyman-Pearson), multiple hypotheses, and coloured noise backgrounds. For instance, the same approach can be applied to the detection of a weak signal adjacent in frequency to a masking signal, securing a pre-specified false alarm rate.

The results form the basis for future investigation into algorithms that utilise cues from temporal fine structure, for example, receivers that maintain phase continuity through transient noise, and systems to automatically group phase tracks.

Acknowledgment

Robert Mill was supported by a studentship funded by the UK Ministry of Defence Research Programme.

References

[1] W. S. Burdic, *Underwater Acoustic Systems Analysis*, 1st ed. Englewood Cliffs, NJ 07632: Prentice-Hall, 1994.

[2] G. M. Wenz, "Acoustic ambient noise in the ocean: Spectra and sources," *J. Acoust. Soc. Amer.*, vol. 34, pp. 1936–1956, 1962.

[3] B. C. J. Moore, *An Introduction to the Psychology of Hearing*, 5th ed. London: Academic Press, 2003.

[4] R. N. McDonough and A. Whalen, *Detection of Signals in Noise*, 2nd ed., R. N. McDonough, Ed. Academic Press, 1995.

[5] J. O. Pickles, *An Introduction to the Physiology of Hearing*, 2nd ed. London: Academic Press, 1988.

[6] D.-S. Kim, S.-Y. Lee, and R. M. Kil, "Auditory processing of speech signals for robust speech recognition in real-world noisy environments," *IEEE Trans. Speech Audio Processing*, vol. 7, pp. 55–69, 1999.

[7] K. Wang and S. Shamma, "Self-normalization and noise-robustness in early au ditory representations," *IEEE Trans. Speech Audio Processing*, vol. 2, no. 3, pp. 421–435, 1994.

[8] O. Ghitza, "Temporal non-place information in the auditory-nerve firing patterns as a front-end for speech recognition in a noisy environment," *J. Phonetics*, vol. 16, pp. 109–123, 1988.

[9] S. C. Sekhar and T. V. Sreenivas, "Auditory motivated level-crossing approach to instantaneous frequency estimation," *IEEE Trans. Signal Processing*, vol. 53, no. 4, pp. 1450–1462, 2005.

[10] T. J. Gardner and M. O. Magnasco, "Sparse time-frequency representations," *Proc. National Academy of Sciences*, vol. 103, no. 16, pp. 6094–6099, 2006.

[11] S. A. Fulop and K. Fitz, "Algorithms for computing the time-corrected instantaneous frequency (reassigned) spectrogram," *J. Acoust. Soc. Amer.*, vol. 119, no. 1, pp. 360–371, 2006.

[12] H. R. Dajani, W. Wong, and H. Kunov, "Fine structure spectrography and its application in speech," *J. Acoust. Soc. Amer.*, vol. 107, no. 6, pp. 3902–3918, 2005.

[13] P. Z. Peebles, Jr., *Probability, Random Variables, and Random Signal Principles*, 3rd ed. McGraw-Hill, 1993.

[14] R. W. Mill, "Statistics of interval receivers in gaussian noise," Department of Computer Science, University of Sheffield, UK, Tech. Rep. CS-07-07, 2007.

[15] S. O. Rice, "Mathematical analysis of random noise," *Bell Systems Tech. J.*, vol. 23, pp. 282–332, 1944.